Imaging of spaceborne ScanSAR with multiple azimuth beams

KOU Guangjie[1,2,3], **WANG Zhensong**[1], **YAO Ping**[1]

1. *Institute of Computing Technology*, *Chinese Academy of Sciences*, *Beijing* 100190, *China*;
2. *Graduate School*, *Chinese Academy of Sciences*, *Beijing* 100049, *China*;
3. *School of Information Science and Engineering*, *Ludong University*, *Shandong Yantai* 264025, *China*

Abstract: This paper proposes a novel work mode of spaceborne ScanSAR with multiple azimuth beams, where the range swath coverage can be greatly extended while the azimuth high resolution remains unchanged. Based on the analysis of the characteristics and main phase errors of this mode, the compensating methods for these errors are given. Then the echo data simulating methods for this mode are introduced and the corresponding imaging algorithms are discussed as well. Thus the feasibility of this mode and the validity of the compensating methods are proved by simulation.

Key words: CS, DPCMAB, RD, ScanSAR, SPECAN

CLC number: TP722.6 **Document code:** A

Citation format: Kou G J, Wang Z S, Yao P. 2010. Imaging of spaceborne ScanSAR with multiple azimuth beams. *Journal of Remote Sensing*. **14**(6): 1105—1116

1 INTRODUCTION

ScanSAR is a wide-swath spaceborne SAR mode. But the performance of wide swath is at the expense of the greatly declined azimuth resolution (Andrea *et al.*, 1996; Eldhuset *et al.*,1995; Jurgen *et al.*,2002). The technique of displaced phase centers multiple azimuth beams (DPCMAB) can improve the azimuth resolution greatly on the premise of maintaining a low pulse repetition frequency (PRF) (Currie *et al.*,1992; Gerhard *et al.*, 2004; Kou *et al.*, 2009). If we combine these two modes, the performance which can not be obtained by single mode is achieved. Based on this idea, a new mode (MAB- ScanSAR) is proposed which adopts six azimuth beams and five elevation subswaths. The overall swath width is extended five times while the same azimuth resolution as conventional stripmap SAR is remained. Firstly, the principle and main phase errors of MAB-ScanSAR are analyzed and the corresponding compensating equations are deduced. Secondly, the raw data simulation methods under different conditions are presented and several imaging algorithms fit for MAB-ScanSAR are discussed too. Lastly, the effectiveness of this mode is proved by simulation.

2 BASIC PRINCIPLE OF MAB-SCANSAR

2.1 Principle of DPCMAB

The essential idea of DPCMAB is to substitute high sampling frequency in space domain for high sampling frequency in time domain. Hence, a higher effective azimuth sampling rate can be obtained for a certain system operating PRF. The system operating PRF is the actual pulse transmitting frequency in SAR system and corresponding to it is the equivalent PRF. If there are N receivers in azimuth direction, then N echoes can be received for every transmitted pulse. From the view of the receiver, the PRF is improved N times and the improved PRF is called equivalent PRF.

Fig. 1 illustrates the antenna principle of six azimuth beams SAR. The transmitter (S) is at the middle of the antenna and the receivers are at its two sides. Assuming the overall antenna length is L, the distances of transmitter to respective receivers are displayed in Fig.1. The left side receivers are denoted by negative sign in the figure. The azimuth aperture is extended six times by the weighted antenna (Doppler bandwidth is broadened six times) when the system works. Meanwhile, the equivalent PRF is improved six times by the six receivers, but the system operating PRF is still kept unchanged. In the end,

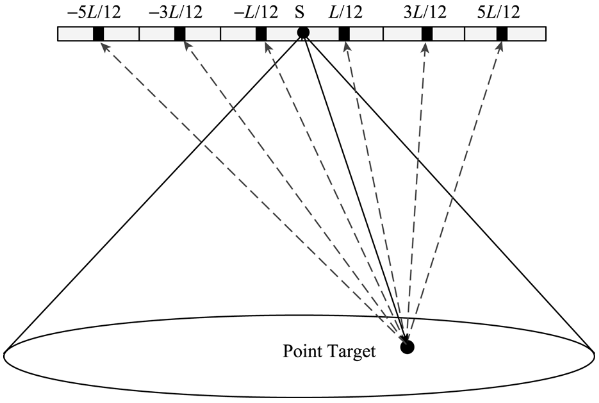

Fig. 1 Antenna principle of six azimuth beams SAR

Received: 2009-10-10; **Accepted**: 2010-06-02

Foundation: The 11th Five-Year Plan national advanced research project.

First author biography: KOU Guangjie(1977—), male, He is currently pursuing the Ph.D. degree at the Institute of Computing Technology, Chinese Academy of Sciences. He majors in simulation of SAR system, SAR signal processing and image processing. E-mail: kouguangjie@ict.ac.cn the azimuth resolution is improved six times than the conventional stripmap SAR.

2.2 Principle of ScanSAR

Fig. 2 displays the principle of a single-look ScanSAR with five subswaths. $T_{\mathrm{D}j}$ is the dwell time of subswath j and it determines the real azimuth resolution. T_{R} is the signal cycle and it is defined as the time interval between the beginnings of two adjacent bursts at a given subswath.

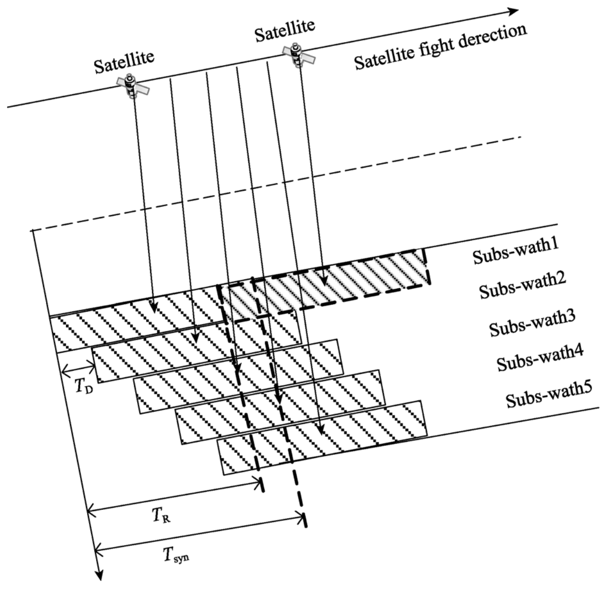

Fig. 2 Principle of five subswaths ScanSAR

Assume T_{syn} expresses the synthetic aperture time of every subswath, to achieve continuous along-track image, the preceding times should satisfy

$$T_{\mathrm{syn}} \geqslant T_{\mathrm{R}} + T_{\mathrm{D}j} \qquad j = 1,\ldots,N_B \tag{1}$$

where N_{B} is total number of subswaths and T_{R} meets Eq.(2).

$$T_{\mathrm{R}} = \sum_{j=1}^{N_B} (T_{\mathrm{D}j} + T_{\mathrm{c}}) \tag{2}$$

where T_c is the beam switching time between subswaths. Assume the dwell times are equal and T_c is neglected (T_{D}>>T_{c}), Eq. (1) can be rewritten as follows.

$$T_{\mathrm{syn}} \geqslant (N_{\mathrm{B}} + 1)T_{\mathrm{D}} \tag{3}$$

Since azimuth resolution ρ_{burst} is determined by real bandwidth $f_{\mathrm{d}r} \cdot T_{\mathrm{D}}$, based on the preceding relations we can obtain the following equation.

$$\rho_{\mathrm{burst}} = \frac{v_g}{f_{\mathrm{d}r} \times T_{\mathrm{D}}} \geqslant \frac{v_g (N_B + 1)}{f_{\mathrm{d}r} \times T_{\mathrm{syn}}} = (N_{\mathrm{B}} + 1)\rho_{\mathrm{strip}} \tag{4}$$

where $f_{\mathrm{d}r}$ is Doppler rate, v_g is the velocity of beam footprint, and ρ_{strip} is the azimuth resolution of conventional stripmap SAR. Eq.(4) shows that the azimuth resolution in the ScanSAR which has N_{B} subswaths will be degraded at least N_{B}+1 times than the corresponding stripmap SAR. But if we ignore the overlap between the subswaths, the overall swath width is extended N_{B} times.

2.3 Principle of MAB-ScanSAR

If five elevation subswaths are adopted in the six azimuth beams SAR, then MAB-ScanSAR proposed in the paper is achieved. The azimuth resolution is improved six times on the premise of maintaining the operating PRF unchanged by six azimuth beams. Meanwhile, the azimuth resolution is degraded six times because of the five subswaths (the resolution is equal to conventional stripmap SAR again) while the overall swath width is extended five times now.

Generalizing MAB-ScanSAR further, the relations of azimuth receivers number N_{R}, elevation subswaths number N_{B}, and performance of the system can be described as following: the swath width can be extended N_{B} times regardless of the value of N_{R}. However, the azimuth resolution will vary with the value of N_{R}. If $N_{\mathrm{R}}=N_{\mathrm{B}}+1$, the same azimuth resolution as stripmap SAR is obtained. If $N_{\mathrm{R}}>N_{\mathrm{B}}+1$, a better azimuth reso- lution than conventional stripmap SAR is achieved. If $N_{\mathrm{R}}<N_{\mathrm{B}}+1$, the resolution is degraded. The choices of N_{R} and N_{B} can be determined by the preceding relations during system design. In spite of different scenarios, the analysis of phase errors is same to the instance discussed in the paper.

3 PHASE ERRERS AND COMPENSATIONS IN MAB-SCANSAR

The process methods of conventional ScanSAR can be used directly in MAB-ScanSAR, if the phase errors due to multiple azimuth beams are corrected.

3.1 Analysis of the phase errors caused by six azimuth beams

Main phase errors due to multiple azimuth beams are differential path error (Kou *et al.*, 2009) and nonuniform sampling error (Currie *et al.*, 1992). Differential path error is caused by the Earth rotation. This error occurs between the real signal propagation path and the equivalent signal propagation path. It has significant effect on the imaging quality in high frequency SAR.

Fig. 3 displays the relative positions of the antenna and the ground target at a certain moment in the six azimuth beams SAR. S_0 is the transmitter phase center, E_i are effective phase centers, R_i are receiver phase centers, P_0 is ground point target's position at current time, A_i are equivalent ground target's position on the rotational Earth when the equivalent single channel SAR locates at E_i, and i = −3, −2, −1, 1, 2, 3 (negative sign denotes left side). The six received echoes in six azimuth beams SAR will be used to mimic six receiving operations of the single beam SAR at the corresponding effective phase center E_i. The movements of antenna and ground point target at each transmitting-receiving are continuous in single beam SAR. However, the phase histories are discontinuous and six echoes are set as one group in six beams SAR. The difference of these phase histories is the basic cause of differential path error. This phase error is generated by the difference between$|S_0P_0R_{\mathrm{i}}|$ and

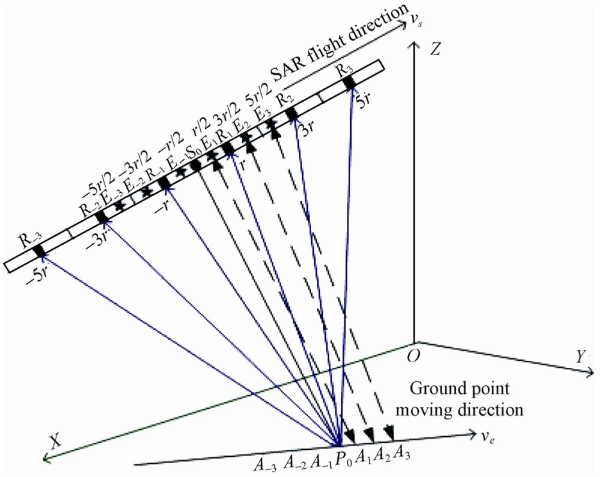

Fig. 3 Differential path error in six azimuth beams SAR

$2|E_iA_i|$ in Fig. 3. They can be approximated by $2|E_iP_0|$-$2|E_iA_i|$, as the difference between $2|E_iP_0|$ and $|S_0P_0R_i|$ can be ignored at all (Currie *et al.*, 1992). To keep the figure clear, only right side equivalent propagation paths are plotted in Fig. 3. The distances of the transmitter to the receivers and the effective phase centers are marked on the figure, where r is half length of the equivalent antenna. If the overall antenna length is L, the equivalent antenna length in six beams SAR is $L/6$ m. As a result $r = L/12$ m.

The nonuniform sampling error means the azimuth nonuniform which the antenna moving distance does not equal to $L/2$ within an interval of pulse repetition. In Fig. 3, this error occurs when the distance between the leftmost effective phase center E_{-3} at next moment and the rightmost effective phase center E_3 at current time does not equal to r. The phase history of multiple beams can be expressed as follows.

$$\phi_a(n) = -4\pi/\lambda R(n\mathrm{PRI}/6) + \phi_{\mathrm{w}}(n) + \phi_{\mathrm{u}}(n) = \\ -4\pi/\lambda R(n\mathrm{PRI}_{\mathrm{e}}) + \phi_{\mathrm{w}}(n) + \phi_{\mathrm{u}}(n) \quad (5)$$

where n=0, 1 , 2, 1⋯ is azimuth pulse number in the equivalent single beam SAR, PRI is system operating pulse repetition interval, $\mathrm{PRI}_{\mathrm{e}}$ is equivalent pulse repetition interval, $\phi_{\mathrm{w}}(n)$ is differential path error, and $\phi_{\mathrm{u}}(n)$ is nonuniform sampling error. Based on the geometry of the satellite and the Earth, $\phi_{\mathrm{w}}(n)$ can be expressed as follows.

$$\phi_{\mathrm{w}}(n) \approx \{[2\,\mathrm{mod}(n,6) - 5]L\pi\omega_{\mathrm{e}} \times \\ R_{\mathrm{e}}\cos\Phi_t \cos\delta\}/(6\lambda v_s) \quad (6)$$

where mod$(n,6)$=0,⋯, 5 denotes the beam number starting from left side, ω_{e} is the Earth rotation velocity, R_{e} is radius of the Earth, Φ_t is latitude of the ground point target, λ is wavelength of radar carrier, v_{s} is satellite velocity, δ is the angle between radar beam and ground target velocity.

$$\cos\delta = (R_{\mathrm{s}}/R_{\mathrm{st}})\sqrt{\cos(\Phi_{\mathrm{s}} + \Phi_{\mathrm{t}}) + \cos\alpha} \times \\ \sqrt{\cos(\Phi_{\mathrm{s}} - \Phi_{\mathrm{t}}) - \cos\alpha}\,/\cos\Phi_{\mathrm{t}} \quad (7)$$

where R_{s} is radius of the satellite orbit, R_{st} is the distance between the satellite and the ground point target, Φ_{s} is latitude of nadir, and α is Earth centre angle (between spacecraft radius vector and scatter location vector).

Azimuth nonuniform sampling error can be compensated by spectrum reconstruction (Kou *et al.*, 2009; Yin, 1997) etc. Certainly, the analytic expression of $\phi_{\mathrm{u}}(n)$ can be written out based on the specific orbit and Earth model and compensated as a phase error. However, the radar satellites nowadays almost all have yaw steering which reduces the effect of nonuniform sampling error significantly. The simulation analysis of the preceding errors is presented in section 6.

3.2 Problems due to scan in elevation

In MAB-ScanSAR, problems due to scan in elevation direction are the same as the conventional ScanSAR. They are the stitching of image blocks inside or outside the subswath, variation of ground resolution in range direction etc.

4 ECHO DATA SIMULATION IN MAB-SCANSAR

A local sphere Earth and circle orbit model is adopted. The geometry relationships are represented by eight coordinates and echo data under different conditions can be generated by the following methods.

4.1 Simulation of yaw steering

Yaw steering is a technique which can maintain the Doppler centric frequency f_{dc} at zero all the time. It is realized by adjusting the yaw angle along the orbit continuously. In simulation, the yaw angles at different orbit positions can be calculated by Eq.(8) (Raney, 1986).

$$\tan a = \varepsilon(\omega_{\mathrm{s}}/\omega_{\mathrm{e}} - \cos\psi)/(\cos\beta\sin\psi) \quad (8)$$

where a is yaw angle, β is satellite latitude, ε=1(−1) denotes radar works in left & right side looking mode, ψ is the orbit inclination angle, ω_{s} is the satellite orbital rotation rate, and ω_{e} is the Earth rotation rate.

4.2 Simulation of multiple azimuth beams

The simulation of six azimuth beams in Fig.3 can be distinguished into following three categories: (1) only differ- rential path error is considered; (2) only nonuniform sampling error is taken into account; (3) both errors are considered. In category (1), the round trip signal propagation distance of i channel is calculated by $|S_0P_0R_i|$, and the idea PRF (the dis- tances of the SAR antenna moving in every pulse repetition interval are equal to $L/2$m) adopted. The round trip signal propagation distance of i channel should be calculated by $2|E_iA_i|$ in category (2). In category (3), the signal propagation distance is calculated as category (1), however, the system operating PRF does not equal to ideal PRF.

4.3 Simulation of the mode with multiple azimuth beams and scan in elevation

Neglecting azimuth phase errors, the point target impulse function generated in section 4.2 of the multiple azimuth beams SAR can be expressed by the equivalent single beam SAR's impulse function (Andrea *et al.*, 1996; Jurgen *et al.*, 2002).

$$h_{\mathrm{SAR}}(\tau,t;r_0,\xi)=W_{\mathrm{a}}\left(\frac{v_S(t-\xi)}{r_0}\right)W_r\left(\tau-\frac{2\Delta R((t-\xi);r_0)}{c}\right)\times$$
$$\exp(-j(\tfrac{4\pi\Delta R((t-\xi);r_0)}{\lambda})) \tag{9}$$

where τ is fast time in range direction, t is slow time in azimuth direction of the equivalent single beam SAR, and (r_0, ξ) is the point target position. If scan mode is adopted, the response function can be expressed as follows.

$$h_{\mathrm{scan}}(\tau,t;r_0,\xi)=h_{\mathrm{SAR}}\times W_{\mathrm{sc}}(t) \tag{10}$$

where $W_{\mathrm{sc}}(t)$ is rectangle function corresponding to the subswath illumination time T_{D}, and can be expressed as follows.

$$W_{\mathrm{sc}}(t)=\sum_k \mathrm{rect}((t-kT_{\mathrm{R}})/T_{\mathrm{D}}) \tag{11}$$

Thus, the echo data simulation of the same subswath in MAB-ScanSAR can be realized as following. At first, the multiple beams stripmap mode echo data corresponding to this subswath is generated where the ScanSAR parameters are adopted. Then, the temporal relation of each subswath is used to intercept the corresponding burst data directly. However, if the overlapping and stitching of adjacent subswaths are simulated, the echo data should be generated by adjusting the antenna direction based on the working process of scan mode.

5 DISCUSSION OF IMAGING ALGORITHMS IN MAB-SCANSAR

5.1 Characteristics comparison of three common ScanSAR imaging algorithms

SPECAN, full aperture RD and full aperture CS are common imaging algorithms in ScanSAR. Among them SPECAN is the first choice for low resolution quick look processing of ScanSAR. Since only linear range migration item is corrected in SPECAN, it is not fit for high resolution imaging (refer to simulation analysis in section 6.1). If SPECAN is used in high resolution imaging, the effect of range curvature should be considered. Thus the priority of high computing efficient is lost. Full aperture algorithm is known as coherent multiple bursts algorithm too. It firstly fills zeros to the gaps of the ScanSAR echo data, and then the common stripmap imaging algorithms is used. The biggest merit of this method is that it can be obtained from conventional stripmap imaging processor easily. But the computing efficiency will be degraded to a certain degree because of the zero padding operation. Furthermore, the image quality is degraded because of the cross modulation among azimuth bursts. For amplitude image, this effect can be restrained by a subsequent low passing filter (Cumming *et al.*, 2005).

5.2 Computational analysis of three imaging algorithms

The flowcharts of processing one subswath in MAB-ScanSAR with the algorithms discussed in section 5.1 are displayed in Fig. 4, where the operation of azimuth phase error compensation is to remove the phase errors introduced by multiple azimuth beams. The subswaths stitching are same to conventional ScanSAR. For the high resolution in MAB-ScanSAR, the effect of range curvature should be considered (refer to section 6.1). Hence, the flowchart of conventional SPECAN (Sack *et al.*, 1985) changes to Fig. 4(c). Although RD algorithm has a simple structure, the small range migration is also required. However, CS algorithm can get accurate imaging result under the condition of big squint angle and big range migration. So, CS is well used in high resolution imaging.

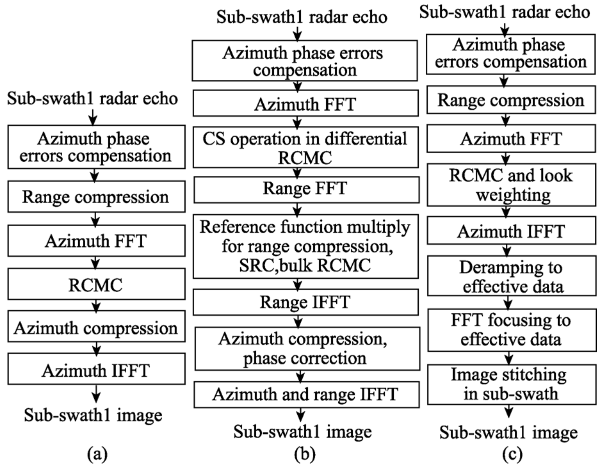
Sub-swath1 radar echo
Azimuth phase errors compensation
Range compression
Azimuth FFT
RCMC
Azimuth compression
Azimuth IFFT
Sub-swath1 image
(a)
Sub-swath1 radar echo
Azimuth phase errors compensation
Azimuth FFT
CS operation in differential RCMC
Range FFT
Reference function multiply for range compression, SRC,bulk RCMC
Range IFFT
Azimuth compression, phase correction
Azimuth and range IFFT
Sub-swath1 image
(b)
Sub-swath1 radar echo
Azimuth phase errors compensation
Range compression
Azimuth FFT
RCMC and look weighting
Azimuth IFFT
Deramping to effective data
FFT focusing to effective data
Image stitching in sub-swath
Sub-swath1 image
(c)

Fig. 4 The flowchart of three imaging algorithms
(a) RD algorithm; (b) CS algorithm; (c) SPECAN algorithm

Using the parameters of section 6.1, the computation comparisons of the preceding three imaging algorithms are listed at below. Since the first steps of phase error compen- sation are the same, they can be neglected when we compare the computation differences. Assume the number of input range lines are N_{az}=65536, the sampling number of each input range line is N_{rg}=16384, the sampling number of each output range line is $N_{\mathrm{rg\_out}}$=15360, and the interpolation kernel M_{ker}=8, then the total number of floating operations in RD can be approximated by (12) (Cumming *et al.*, 2005).

$$\begin{aligned}\mathrm{FLOP}_{\mathrm{RD}}&=5N_{\mathrm{rg}}N_{\mathrm{az}}\log_2 N_{\mathrm{rg}}\times 2+6N_{\mathrm{rg}}N_{\mathrm{az}}+6N_{\mathrm{rg\_out}}N_{\mathrm{az}}+\\&\quad 5N_{\mathrm{rg\_out}}N_{\mathrm{az}}\log_2 N_{\mathrm{az}}\times 2+2(2M_{\mathrm{ker}}-1)N_{\mathrm{rg\_out}}N_{\mathrm{az}}=\\&\quad 354.0664\ (\mathrm{GFLOP})\end{aligned} \tag{12}$$

The total number of floating operations in CS is

$$\begin{aligned}\mathrm{FLOP}_{\mathrm{CS}}&=5N_{\mathrm{rg}}N_{\mathrm{az}}\log_2 N_{\mathrm{rg}}\times 3+6N_{\mathrm{rg}}N_{\mathrm{az}}\times 2+\\&\quad 6N_{\mathrm{rg\_out}}N_{\mathrm{az}}+5N_{\mathrm{rg\_out}}N_{\mathrm{az}}\log_2 N_{\mathrm{az}}=\\&\quad 324.9411\ (\mathrm{GFLOP})\end{aligned} \tag{13}$$

Assume the processing length of each burst is N_{Burst}=8192, even if the floating operations of image stitching and phase errors compensation are neglected, the additional floating operations of SPECAN (Fig. 4(c)) relative to RD still can be expressed as

$$\begin{aligned}\mathrm{FLOP}_{\mathrm{add}}&=6N_{\mathrm{rg\_out}}N_{\mathrm{Burst}}\times 2+\\&\quad 5N_{\mathrm{rg\_out}}N_{\mathrm{Burst}}\log_2 N_{\mathrm{Burst}}\times 2=\\&\quad 17.8677\ (\mathrm{GFLOP})\end{aligned} \tag{14}$$

Preceding comparisons show that CS algorithm has superiority in MAB-ScanSAR on computation too. Certainly, the choice of specific algorithm should give an integrated consideration of the already existing imaging processors and the computing complexity etc.

6 SIMULATION ANALYSIS

Nowadays, almost all radar satellites have yaw steering which can reduce azimuth phase errors effectively and simplify the signal processing. So yaw steering is added to all the simulations in the paper. Other main parameters are listed in Table 1.

Table 1 Simulation parameters

Satellite height/km	800	Ideal PRF/Hz	1656
Orbit inclination angle/°	98.6	Subswath1 PRF /Hz	1680
Antenna length/m	9	Subswath2 PRF /Hz	1665
Wavelength/m	0.05656	Subswath3 PRF/Hz	1680
Bandwidth/MHz	33	Subswath4 PRF/Hz	1665
Sampling frequency /MHz	40	Subswath5 PRF/Hz	1680
Pulse duration /μs	20		

6.1 Simulation analysis of high resolution SPECAN

To ensure the imaging quality, whether to correct the range curvature should be analyzed when SPECAN is used to form high resolution image. As an example, if parameters in Table 1 are used to analyze the first subswath. The range curvature in MAB-ScanSAR can be approximated by Eq. (15) (Curlander *et al.*, 1991). The range curvature is 152.5 m (about 5.5 gates) even in a burst when the satellite is over the equator and the look angle is 30°. Thus, the effect of range curvature can not be ignored already.

$$R_{\text{square}} = \frac{\lambda|f_{\text{d}r}|}{4}(t-t_0)^2 \approx \frac{\lambda|f_{\text{d}r}|}{4}\left(\frac{\lambda \cdot R_c}{2Dv_s}\right)^2 \tag{15}$$

where t_0 is the time when the center of the radar beam crosses the target, R_c is the beam length, D is the equivalent antenna length, v_s is the satellite velocity. The imaging results of a burst formed by SPECAN are displayed in Fig.5 where the differential path error is removed. Fig.5(a)(b) are imaging results when the range curvature is included in range migration correction (RCMC). The azimuth 3dB resolution is 4.5 m and the slant range 3 dB resolution is 4.6 m. So, the point target is focused well. If the range curvature is neglected, the decoupling in range and azimuth direction can not be achieved and the point target can not be focused. The profile maps along azimuth and range direction are displayed in Fig.5(c)(d), where the azimuth 3 dB resolution changes to 9.3 m, the slant range 3 dB resolution changes to 6.3 m and the left sidelobe is higher than −7.5 dB. Hence, simulation results prove that range curvature must be considered in RCMC when the parameters in Table 1 are used. Thus, the superiority of SPECAN relative to full aperture RD or CS does not exist now.

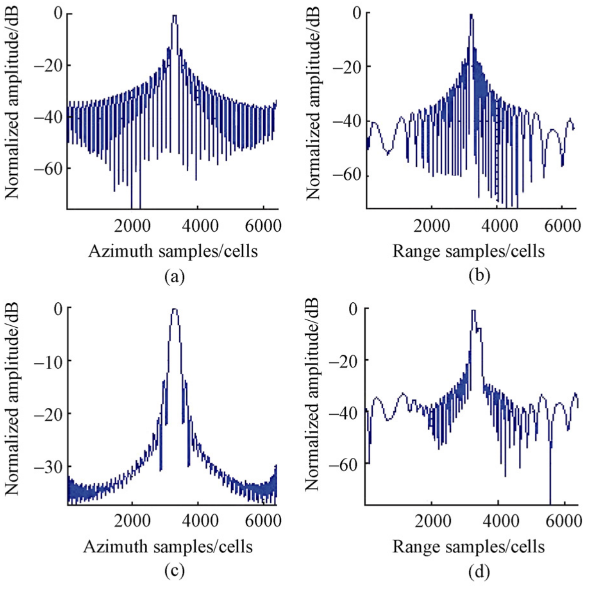

Fig. 5 SPECAN imaging results

(a) Azimuth profile map with accurate RCMC; (b) Range profile map with accurate RCMC; (c) Azimuth profile map when the range curvature is ignored; (d) Range profile map when the range curvature is ignored

Since the abscissas are interpolated 64 times in Fig. 5, the range sampling spacing is 4.55/64=0.07 m and azimuth sampling spacing of SPECAN can be determined by Eq. (16) (Cumming *et al.*, 2005).

$$\delta_{\text{a}} = \frac{v_{\text{s}} \times PRF_{\text{e}}}{64 \cdot N_{\text{fft}}/|f_{\text{d}r}|} \tag{16}$$

where v_{s} is the velocity of satellite, PRF_{e} is the equivalent PRF, N_{fft} is the FFT length of the focusing operation in SPECAN, $f_{\text{d}r}$ is the Doppler rate. In the instance, v_{s} is 7451.8 m/s, PRF_{e} is 10080 Hz, N_{fft} is 16384 points, $|f_{\text{d}r}|$ is 1890.9 Hz/s, so the azimuth sampling interval is 0.04 m. The normalized amplitude coordinates is calculated by 20log ($f/f_{\max}$) in the paper, where $f_{\max}$ is the maximum amplitude, f is real amplitude of the samples.

6.2 Simulation analysis of phase errors caused by multiple azimuth beams

The process of MAB-ScanSAR is same to ScanSAR, if the azimuth phase errors are compensated well or the effects of these phase errors can be ignored. Different azimuth phase errors are generated by the methods of section 4.2 and the imaging analysis is done by CS algorithm. To avoid cross modulation among the bursts, the imaging operation is only applied on the effective burst when the point target is analyzed. Because of yaw steering, the effect of nonuniform sampling error becomes marginal and the variation is small along the orbit. For example, when the parameters of Table 1 and the data of first subswath are used, the maximum false target amplitude is only about −42.5 dB (Fig.6(c)) even if the system operating PRF deviates from ideal PRF (1656 Hz) 200 Hz (corresponding PRF_{e} is 11136 Hz). Thus, the effect of this error on imaging quality can be ignored at all.

The effect of differential path error is changed greatly along the orbit because of the Earth rotation. Simulation results are displayed in Fig.6 when the satellite at 35°N where the effect of differential path error becomes serious.

The azimuth profile map with combined phase errors is displayed in Fig.6(a) and the maximum amplitude of the false target becomes −9 dB. The false targets are removed effectively by Eq. (6), SNR has also been greatly improved and the result is plotted in Fig.6(b). The imaging result only with nonuniform sampling error is displayed in Fig.6(c). The comparision between Fig.6(b) and Fig.6(c) shows that the residual false targets in Fig.6(b) are mainly caused by nonuniform sampling error and the effect to imaging quality can be neglected. For the convenience of analysis the imaging results without both phase errors is displayed in Fig. 6(d). The sampling spacing of the abscissas is $v_{\text{s}}/PRF_{\text{e}}$=0.67m in Fig. 6.

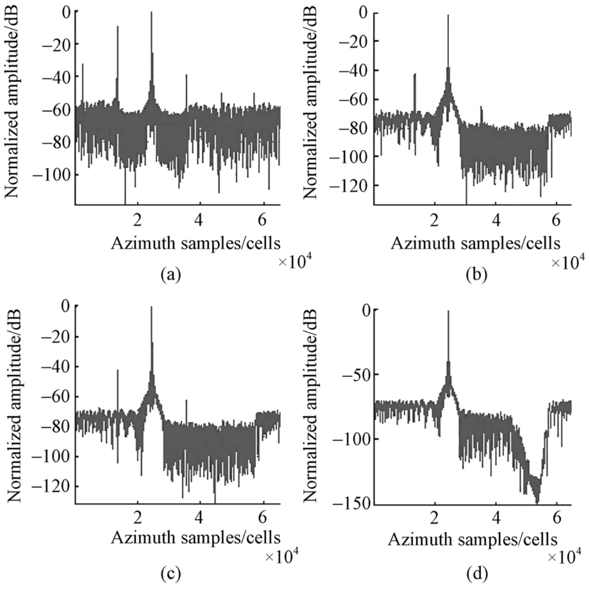

Fig. 6 Simulation analysis of phase errors at 35°N

(a) With both phase errors; (b) Compensated differential path error of (a); (c) Only with nonuniform sampling error; (d) Without phase errors

6.3 Comparative analysis of imaging results in MAB-ScanSAR

The point target image results of stripmap mode, ScanSAR mode and MAB-ScanSAR (after compensating differential path error) are presented in Fig.7, where the look angle is 30°, system operating PRF is 1680 Hz, and the satellite is over the equator. Furthermore, the scan mode is single look and five subswaths.

The horizontal direction is the azimuth direction in Fig.7. For convenience of comparison the azimuth sampling spacing is unified to v_s/PRF=4.44 m, and the sampling spacing in range direction is 4.55 m. The quantitative indexes of the preceding imaging results are summarized in Table 2.

Table 2 Imaging performance comparison of different modes

Work mode	ρ_r/m	ρ_a/m	Overall swath width/km
Stripmap mode	4.6	4.5	69.2
Scan mode	4.6	27	346
MAB-ScanSAR	4.6	4.5	346

In Table 2, ρ_r is slant range 3 dB resolution, ρ_a is azimuth 3dB resolution. The overall swath width denotes the optimal width when the overlap between the subswaths is neglected. Considering the subswath overlaps and the subswath stitching in real system, the real overall swath width is less than preceding value (Jurgen *et al.*, 2002; Cumming *et al.*, 2005). The simulation results show that MAB-ScanSAR can extend the swath width 5 times and keep the azimuth resolution same as stripmap mode under ideal condition.

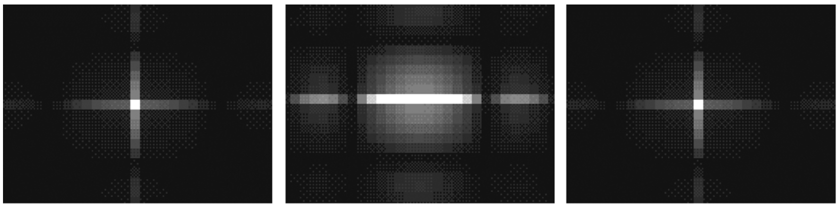

(a) (b) (c)

Fig. 7 Grayscale images of point target for three work mode

(a) Stripmap mode; (b) Scan mode; (c) MAB-ScanSAR mode

7 CONCLUSIONS

To achieve wider swath width and keep the high azimuth resolution unchanged, a new work mode MAB-ScanSAR is proposed in the paper. The optimal theory performance is given. Based on the analysis of the main phase errors, the specific compensation methods are presented and several imaging algorithms suitable for this mode are studied too. The effectiveness and feasibility of the proposed methods are proved by the point target simulation.

REFERENCES

Andrea M G and Claudio P. 1996. ScanSAR focusing and interferometry. *IEEE Transaction on Geoscience and Remote Sensing*, **34**(4): 1029—1038

Cumming I G and Wong F H. 2005. Digital Processing of Synthetic Aperture Radar Data: Algorithms and Implementation. Norwood: Artech House Inc

Curlander J C and Mcdonough R N.1991.Synthetic Aperture Radar: Systems and Signal Processing. New York: Wiley & Sons, Inc.

Currie A and Brown M A. 1992. Wide-swath SAR. *IEE Proceedings-F*, **139**(2): 122—135

Eldhuset K and Valand P A. 1995. ScanSAR processing and simulation for ASAR using ERS-1 raw data. *Intentional Journal of Remote Sensing*, **16**(14): 2657—2674

Gerhard K, Nicolas G and Alberto M. 2004. Unambiguous SAR signal reconstruction from nonuniform displaced phase center sampling. *IEEE Geoscience and Remote Sensing Letters*, **1**(4): 260—264

Jurgen H and Richard B. 2002. Burst mode and ScanSAR interferometry. *IEEE Transaction on Geoscience and Remote Sensing*, **40**(9): 1917—1934

Kou G J, Wang Z S and Yao P. 2009. Study on signal processing of azimuth multi-channel spaceborne SAR with yaw steering. IET International Radar Conference 2009, Guilin, China

Raney R K. 1986. Doppler properties of radars in circular orbits. *Intentional Journal of Remote Sensing*, **7**(9): 1153—1162

Sack M, Ito M R and Cumming I G.1985. Application of efficient linear FM matched filtering algorithms to synthetic aperture radar processing. IEEE Proceedings. **132**(1): 45—57

Yin C J.1997.Perfect reconstruction of digital spectrum from nonuniformly sampled signals. *IEEE Transaction on Instrumentation and Measurement*, **46**(3): 649—652

星载方位多波束 ScanSAR 成像

寇光杰[1,2,3], 王贞松[1], 姚　萍[1]

1. 中国科学院计算技术研究所　北京 100190;
2. 中国科学院研究生院　北京 100049;
3. 鲁东大学 信息科学与工程学院　山东 烟台 264025

摘　要: 提出了一种新型星载方位多波束 ScanSAR 工作模式, 实现了在保持方位向高分辨率的前提下对距离向测绘带大幅扩展。分析了该工作方式的特点及主要相位误差, 给出了相应的误差补偿方法。介绍了该工作方式下回波数据的模拟方法, 并讨论了几种适合该工作方式的成像算法。最后通过仿真对该工作方式的可行性及补偿方法的有效性进行了验证。

关键词: CS; 分离相位中心方位多波束; 距离多普勒算法; ScanSAR; SPECAN

中图分类号: TP722.6　　**文献标志码:** A

引用格式: 寇光杰, 王贞松, 姚　萍. 2010. 星载方位多波束 ScanSAR 成像. 遥感学报, **14**(6): 1105—1116
Kou G J, Wang Z S, Yao P. 2010. Imaging of spaceborne ScanSAR with multiple azimuth beams. *Journal of Remote Sensing*. **14**(6): 1105—1116

1 引　言

ScanSAR 是星载 SAR 宽测绘带的一种工作模式。但这种宽测绘带性能是以方位向分辨率的大幅下降为代价的(Andrea 等, 1996; Eldhuset 等,1995; Jurgen 等, 2002)。分离相位中心方位多波束(DPCMAB)技术可以在保持较低脉冲重复频率(PRF)的前提下, 获得方位向分辨率的大幅度提高(Currie 等, 1992; Gerhard 等, 2004; Kou 等, 2009)。若将这两种工作方式相结合则可望获得单一工作方式无法得到的性能。基于此想法提出了一种方位向六波束距离向五扫描子带的新型工作模式(MAB-ScanSAR), 该工作模式可以在保持方位向分辨率与常规条带式 SAR 相同的前提下, 获得总测绘带 5 倍展宽的效果。

2 MAB-ScanSAR 基本原理

2.1 DPCMAB 原理

DPCMAB 的本质是通过方位向空间维采样率的增加换取时间维采样率的下降, 在一定的系统工作 PRF 下得到更高的方位向等效采样率。其中系统工作 PRF 是指系统实际发射脉冲的重复频率, 与之相对应的是等效 PRF。若沿方位向有 N 个接收相位中心, 则每发送一个脉冲就可同时接收到 N 个脉冲, 从接收的角度看, 相当于脉冲重复频率提高了 N 倍, 这一提高的脉冲重复频率称为等效 PRF。

图 1 给出了一种方位向六波束 SAR 天线原理。其中发送相位中心(S)位于天线中心, 各接收相位中心位于两侧, 设天线总长为 L, 则各接收相位中心到发送相位中心的距离如图 1, 左侧接收相位中心用负值表示。系统工作时, 一方面通过天线加权使天线方位向波束宽度展宽为原来的 6 倍, 即多普勒带宽展宽 6 倍。另一方面通过六个通道接收数据, 可在系统实际工作 PRF 不变的情况下, 获得原来 6 倍的等效采样率。最终得到方位向分辨率相对常规条带式 SAR 的 6 倍提升。

2.2 ScanSAR 原理

图 2 给出了距离向五扫描子带单视模式 ScanSAR 工作原理。其中 T_{Dj} 为波束在第 j 子测绘带内的驻留时间, 它决定了方位向实际分辨率; T_R 为信号周期,

---

收稿日期: 2009-10-10; 修订日期: 2010-06-02

基金项目: 国家十一五预研项目。

第一作者简介: 寇光杰(1977—　), 男, 中国科学院计算技术研究所博士研究生, 目前主要从事 SAR 系统仿真, SAR 成像及图像处理等方面的研究。 E-mail: kouguangjie@ict.ac.cn。

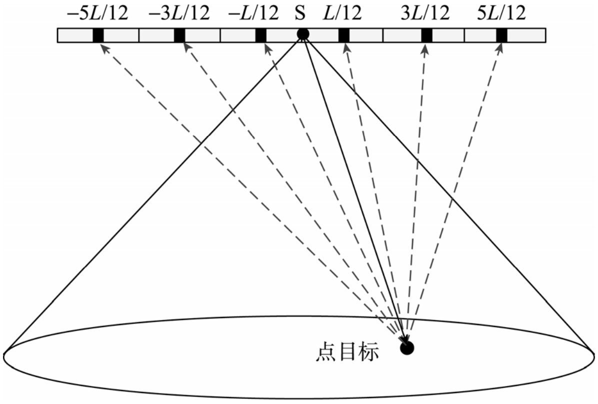

图 1 方位向六波束 SAR 天线原理

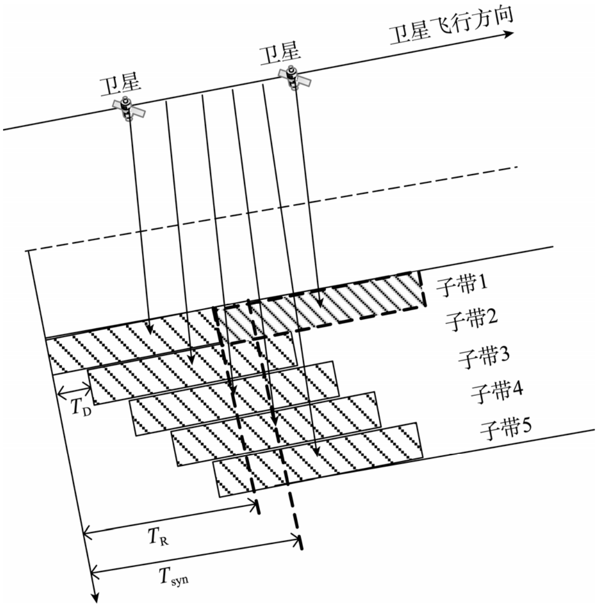

图 2 五扫描子带的 ScanSAR 原理

即同一子带内相邻两个 Burst 起始时间间隔。

若用 T_{syn} 统一表示各子带合成孔径时间，为了保证同一子观测带上相邻图像之间的衔接，以上时间应该满足

$$T_{\text{syn}} \geqslant T_{\text{R}} + T_{\text{D}j} \qquad j = 1, \ldots, N_B \tag{1}$$

式中，N_B 为子带总数，且 T_{R} 满足式(2)。

$$T_{\text{R}} = \sum_{j=1}^{N_B} (T_{\text{D}j} + T_{\text{c}}) \tag{2}$$

式中，T_{c} 为波束在子带之间的切换时间。若取各个子带的波束驻留时间相同，又因为 $T_{\text{D}} >> T_{\text{c}}$，则忽略 T_{c} 后(1)式可写为

$$T_{\text{syn}} \geqslant (N_B + 1) T_{\text{D}} \tag{3}$$

而方位向分辨率 ρ_{burst} 取决于处理器实际带宽 $f_{\text{d}r} \times T_{\text{D}}$，则根据上述关系可得

$$\rho_{\text{burst}} = \frac{v_{\text{g}}}{f_{\text{d}r} \times T_{\text{D}}} \geq \frac{v_{\text{g}}(N_B+1)}{f_{\text{d}r} \times T_{\text{syn}}} = (N_B + 1)\rho_{\text{strip}} \tag{4}$$

式中 $f_{\text{d}r}$ 为多普勒调频率，v_{g} 为波束在地面移动速度，ρ_{strip} 为常规条带式 SAR 方位向分辨率。由式(4)可知，对于 N_B 个子带的情况，扫描模式方位向分辨率至少下降为其对应条带模式的 N_B+1 倍。不过，若忽略子带间重叠，此时可使总测绘带展宽 N_B 倍。

2.3 MAB-ScanSAR 原理

若在方位向六波束 SAR 系统中，距离向上采用 5 个子带扫描的方式，就得到了本文所提出的 MAB-ScanSAR 工作模式。该模式一方面通过方位向六波束，可以在不提高系统工作 PRF 的前提下，将方位向分辨率提升 6 倍；另一方面通过 5 个子带扫描又使方位向分辨率下降 6 倍(又变成与常规条带式 SAR 方位向分辨率相同)，但此时总测绘带却获得了 5 倍的展宽。

若将 MAB-ScanSAR 推广，得到方位向接收通道数 N_{R}、距离向扫描子带数 N_B 和系统性能之间的关系如下：不论 N_{R} 取何值，测绘带宽均可展宽 N_B 倍，但方位向分辨率会随 N_{R} 取值的不同有所变化。若 $N_{\text{R}}=N_B+1$ 则方位向分辨率将与常规条带式 SAR 相同；若 $N_{\text{R}}>N_B+1$，则方位向分辨率相对常规条带式 SAR 会有提高；若 $N_{\text{R}}<N_B+1$，则方位分辨率会有下降。进行系统设计时，根据上述关系和实际的需要决定 N_{R}、N_B 的具体取值。虽然会有不同的组合，但相位误差的分析与文中例子相同。

3 MAB-ScanSAR 的误差

校正了方位向多波束引入的相位误差，MAB-ScanSAR 的数据处理采用普通 ScanSAR 的处理方法。

3.1 方位向六波束引起的误差

方位向多波束会造成方位向传播路径误差(Kou 等，2009)和非均匀采样误差(Currie 等，1992)。其中传播路径误差是指因地球自转引起实际脉冲传播路径和等效传播路径之间的误差，该误差对高频段 SAR 成像质量的影响较为明显。

图 3 给出了某一时刻方位向六波束天线及地面目标之间的相对位置关系。其中 S_0 为发送相位中心，E_i 为等效相位中心；R_i 为接收相位中心；P_0 为当前时刻地面点目标所处位置；由于地球是转动的，A_i 为等效单波束 SAR 位于空中 E_i 位置时地面点目标 P_0 所处位置。其中 i= −3, −2, −1, 1, 2, 3，负值表示左侧。方位向六波束 SAR 每次接收到的 6 个数据，分别用

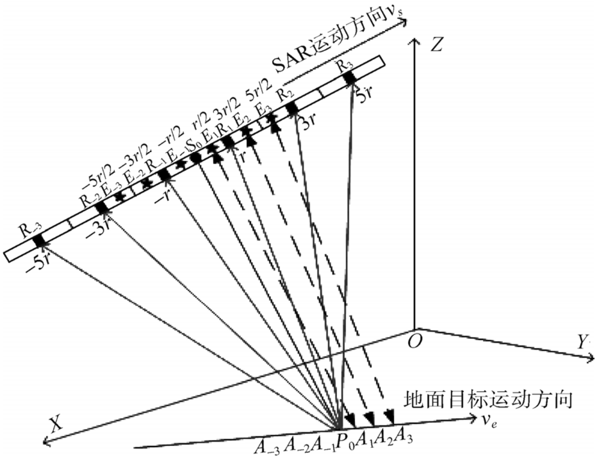
SAR运动方向v_s
Z
R_3
$5r$
$-5r/2$ $-3r/2$ $-r/2$ $r/2$ $3r/2$ $5r/2$
R_{-2} E_{-3} E_{-2} R_{-1} E_{-1} S_0 E_1 R_1 E_2 E_3 R_2
r
$3r$
$-r$
$-3r$
R_{-3}
$-5r$
O
Y
X
地面目标运动方向
v_e
A_{-3} A_{-2} A_{-1} P_0 A_1 A_2 A_3

图 3　方位向六波束 SAR 的传播路径误差

来模拟 6 倍 PRF 单波束 SAR 位于相应等效相位中心 E_i 处的 6 次接收。单波束 SAR 每次发送接收时天线及地面点目标是连续运动的，而六波束 SAR 中是 6 个数据一组跳跃式的相位历程，正是这种相位历程的差异形成了传播路径误差。在图 3 中就是指 $|S_0P_0R_i|$与 $2|E_iA_i|$之间的差值所造成的相位误差。它们可以通过求 $2|E_iP_0|$和 $2|E_iA_i|$之间的差异来近似，通过泰勒展开可以证明 $2|E_iP_0|$与$|S_0P_0R_i|$之间的差异可忽略(Currie 等，1992)。为图形清晰起见，图 3 中只画出了右侧的等效传播路径。各接收相位中心和等效相位中心到发送相位中心的距离已经标出。其中 r 为等效天线长度的一半，若天线物理长度为 L，则六波束 SAR 中等效天线长为 $L/6$，所以 $r = L/12$。

非均匀采样误差是在一个脉冲重复间隔时间内，天线移动的距离不等于 $L/2$ 时产生的方位向采样误差。在图 3 中就是指下一时刻的最左侧等效相位中心 E_{-3} 到当前时刻最右侧等效相位中心 E_3 的间隔不再等于 r 时出现的误差。多波束工作方式下，方位向相位历程可表示为

$$\begin{aligned}\phi_a(n) &= -4\pi/\lambda R(n\mathrm{PRI}/6) + \phi_\mathrm{w}(n) + \phi_\mathrm{u}(n) = \\ &\quad -4\pi/\lambda R(n\mathrm{PRI}_\mathrm{e}) + \phi_\mathrm{w}(n) + \phi_\mathrm{u}(n)\end{aligned} \tag{5}$$

式中，n=0, 1, 2, …为等效单波束 SAR 的方位向脉冲号；PRI 为系统工作脉冲重复间隔时间；PRI_e为等效脉冲重复间隔时间；$\phi_\mathrm{w}(n)$为传播路径误差；$\phi_\mathrm{u}(n)$为非均匀采样误差。根据星地几何关系，可推导出$\phi_\mathrm{w}(n)$为

$$\begin{aligned}\phi_\mathrm{w}(n) \approx \{[2\,\mathrm{mod}(n,6)-5]L\pi\omega_\mathrm{e} \times \\ R_\mathrm{e}\cos\varPhi_t\cos\delta\}/(6\lambda v_\mathrm{s})\end{aligned} \tag{6}$$

式中，$\mathrm{mod}(n,6)=0,\cdots,5$ 表示从左侧起的波束号。ω_e为地球自转角速度，R_e为地球半径，$\varPhi_\mathrm{t}$为地面点目标所在纬度，λ为雷达脉冲信号波长，v_s为卫星速度，δ为雷达视线与点目标运动轨迹夹角。

$$\begin{aligned}\cos\delta = (R_\mathrm{s}/R_\mathrm{st})\sqrt{\cos(\varPhi_\mathrm{s}+\varPhi_\mathrm{t})+\cos\alpha} \times \\ \sqrt{\cos(\varPhi_\mathrm{s}-\varPhi_\mathrm{t})-\cos\alpha}\,/\cos\varPhi_\mathrm{t}\end{aligned} \tag{7}$$

式中，R_s为卫星到地心距离，R_st为雷达视线长度，$\varPhi_\mathrm{s}$为星下点纬度，α为卫星与成像点所夹地心角。

方位向非均匀采样误差可采用频谱重构(Kou 等，2009; Yin,1997)等方法进行均匀化处理。结合特定的轨道和地球模型，可将$\phi_\mathrm{u}(n)$的解析表达式直接写出来，然后作为一个误差相位进行补偿。目前雷达卫星基本具有精确的偏航控制功能，使得非均匀采样误差的影响变得很小。

3.2　距离向扫描引起的问题

MAB-ScanSAR 系统中，距离向扫描引起的问题与普通 ScanSAR 一样。包括子带之间以及子带内部各图像块之间的拼接；距离向地面分辨率不一致等问题。

4　MAB-ScanSAR 回波数据模拟

采用局部地球近似圆球和轨道近似圆形的模型。利用 8 个坐标系表示星地几何关系。根据不同的模拟条件，利用下面相应方法即可生成所需回波数据。

4.1　偏航控制的模拟

偏航控制是通过在轨道不同位置不断调整偏航角使多普勒中心频率 f_dc 的值始终为零的一种技术。在模拟时不同轨道位置处的偏航角可由(8)式求得(Raney,1986)。

$$\tan a = \varepsilon(\omega_\mathrm{s}/\omega_\mathrm{e} - \cos\psi)/(\cos\beta\sin\psi) \tag{8}$$

式中，a 为偏航角；β为卫星纬度；ε为+1, −1 分别表示雷达左右侧视；ψ为轨道倾角；ω_s为卫星沿轨道转动的角速度；ω_e为地球自转角速度。

4.2　方位多波束的模拟

对图 3 所示方位向六波束的模拟可分成以下 3 种情况：(1)只考虑传播路径误差；(2)只考虑非均匀采样误差；(3)同时考虑这两中误差。在(1)中，第 i 通道信号往返传播距离由$|S_0P_0R_i|$计算，并取 PRF 为理想 PRF (在每个脉冲重复间隔时间内 SAR 天线移动距离等于 $L/2$)。对于(2)的模拟，第 i 通道信号往返传播距离应采用 $2|E_iA_i|$。(3)中信号传播距离按照(1)方式计算，系统工作 PRF 不再取理想 PRF。

4.3　方位多波束加距离向扫描模式的模拟

忽略方位向相位误差后，4.2 节所生成的方位多

波束点目标的冲击响应函数，可用等效单波束 SAR 的冲击响应表示(Andrea 等, 1996; Jurgen 等, 2002)。

$$h_{\mathrm{SAR}}(\tau,t;r_0,\xi)=W_{\mathrm{a}}\left(\frac{v_{\mathrm{s}}(t-\xi)}{r_0}\right)W_r\left(\tau-\frac{2\Delta R((t-\xi);r_0)}{c}\right)\times \exp\left(-j\left(\frac{4\pi\Delta R((t-\xi);r_0)}{\lambda}\right)\right) \tag{9}$$

式中，τ为距离向快时间，t 为等效单波束 SAR 方位向慢时间；(r_0, ξ)为点目标位置。采用扫描模式后响应函数为

$$h_{\mathrm{scan}}(\tau,t;r_0,\xi)=h_{\mathrm{SAR}}\cdot W_{\mathrm{sc}}(t) \tag{10}$$

式中，$W_{\mathrm{sc}}(t)$为对应子带照射时间 T_{D} 的矩形窗函数，可表示为

$$W_{\mathrm{sc}}(t)=\sum_k \mathrm{rect}((t-kT_{\mathrm{R}})/T_{\mathrm{D}}) \tag{11}$$

因此，对于同一子带内 MAB-ScanSAR 数据的模拟，首先按照所选用的 ScanSAR 参数生成对应该子带的条带式多波束原始数据，然后按照各子带之间的时序关系直接截取对应位置处的 Burst 数据即可。但是若要仿真子带之间的重叠和拼接，需根据扫描模式的工作过程，通过调整天线指向产生相邻子带的原始数据。

5 MAB-ScanSAR 成像算法讨论

5.1 3 种常用 ScanSAR 成像算法特点比较

SPECAN 算法，全孔径 RD，全孔径 CS 是 ScanSAR 常用的成像算法。其中 SPECAN 算法最适合低分辨率 ScanSAR 的快视处理。该算法只能校正距离线性走动，对于高分辨成像不适合(见 6.1 节仿真分析)。若用于高分辨成像则需要在距离迁徙校正时考虑二次距离弯曲的影响，这样其运算效率高的优势将不存在。全孔径方法又称相干多 Burst 算法，它对 ScanSAR 数据间隙补零，然后采用条带模式的成像算法进行处理。其最大优点是可以很方便的由条带式成像处理器改造而成。因为进行了补零，故效率有所降低，并且在方位向Burst之间存在交叉调制现象，会使图像质量下降。对于幅度图像通过后续低通滤波来抑制交叉调制产生的影响(Cumming 等, 2005)。

5.2 3 种成像算法的运算量分析

图 4 给出了采用 5.1 节 3 种成像算法对 MAB-ScanSAR 系统中一条子带处理流程，其中方位向相位补偿操作用来消除方位多波束引入的相位误差。子带间拼接与常规 ScanSAR 方法一样。本文 MAB-ScanSAR 系统因分辨率较高，所以二次距离弯曲造成的影响已不可忽略(见 6.1 节分析)，这样传统 SPECAN 算法(Sack 等, 1985)的流程图变为图 4(c)。RD 算法虽然结构简单，但也要求距离迁徙不能太大。而 CS 算法，可以对大斜视角及大距离迁徙情况下进行精确成像，所以该算法在高分辨成像时经常选用。

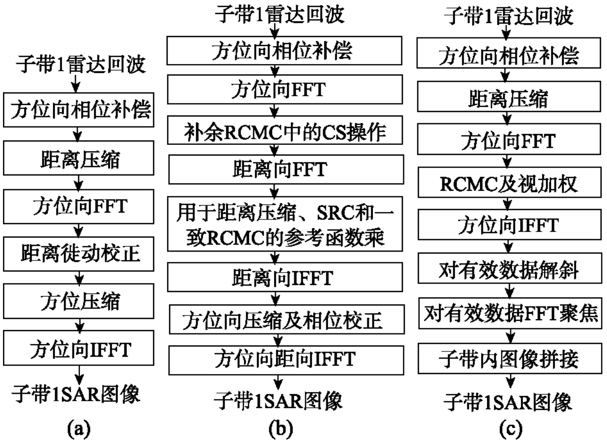

图 4 3 种成像算法的处理流程

(a) RD 算法; (b) CS 算法; (c) SPECAN 算法

以下为参照 6.1 节所选雷达参数，对上述 3 种成像算法的运算量比较。因为 3 种算法中，第一步方位向相位补偿是一样的，所以在比较算法间运算量差别时可以将其略去。假定输入距离线数 N_{az}=65536；每一输入距离线上采样点数 N_{rg}=16384；每一输出距离线上的采样点数 $N_{\mathrm{rg\_out}}$=15360；所用插值核 M_{ker}=8。则 RD 算法所需总浮点运算次数可由(12)式估算(Cumming 等, 2005)。

$$\begin{aligned}\mathrm{FLOP_{RD}}&=5N_{\mathrm{rg}}N_{\mathrm{az}}\log_2 N_{\mathrm{rg}}\times 2+6N_{\mathrm{rg}}N_{\mathrm{az}}+6N_{\mathrm{rg\_out}}N_{\mathrm{az}}+\\&\quad 5N_{\mathrm{rg\_out}}N_{\mathrm{az}}\log_2 N_{\mathrm{az}}\times 2+2(2M_{\mathrm{ker}}-1)N_{\mathrm{rg\_out}}N_{\mathrm{az}}=\\&\quad 354.0664\ (\mathrm{GFLOP})\end{aligned} \tag{12}$$

CS 算法的总浮点运算次数为

$$\begin{aligned}\mathrm{FLOP_{CS}}&=5N_{\mathrm{rg}}N_{\mathrm{az}}\log_2 N_{\mathrm{rg}}\times 3+6N_{\mathrm{rg}}N_{\mathrm{az}}\times 2+\\&\quad 6N_{\mathrm{rg\_out}}N_{\mathrm{az}}+5N_{\mathrm{rg\_out}}N_{\mathrm{az}}\log_2 N_{\mathrm{az}}=\\&\quad 324.9411\ (\mathrm{GFLOP})\end{aligned} \tag{13}$$

若取每个 Burst 处理长度 N_{Burst}=8192，则即使忽略图像拼接所需浮点运算量，并不做相位补偿，图 4(c)中SPECAN算法仍比RD算法多出以下浮点运算量。

$$\begin{aligned}\mathrm{FLOP_{add}}&=6N_{\mathrm{rg\_out}}N_{\mathrm{Burst}}\times 2+\\&\quad 5N_{\mathrm{rg\_out}}N_{\mathrm{Burst}}\log_2 N_{\mathrm{Burst}}\times 2=\\&\quad 17.8677\ (\mathrm{GFLOP})\end{aligned} \tag{14}$$

通过上述比较看出，在 MAB-ScanSAR 系统中 CS 算法在运算量上也有优势。当然具体选用哪种算法还需要结合当前已有的成像处理器、算法复杂度等综合考虑。

6 仿真分析

因目前雷达卫星基本都含有偏航控制功能，而该功能可有效降低方位向相位误差，简化信号处理，

故本文仿真均附加了偏航控制条件，其他主要参数如表 1。

表 1　仿真参数

卫星高度/km	800	理想 PRF/Hz	1656
轨道倾角/(°)	98.6	第一子带 PRF/Hz	1680
天线长度/m	9	第二子带 PRF/Hz	1665
波长/m	0.05656	第三子带 PRF/Hz	1680
带宽/MHz	33	第四子带 PRF/Hz	1665
采样率/MHz	40	第五子带 PRF/Hz	1680
脉冲宽度/μs	20		

6.1　高分辨率 SPECAN 的仿真分析

若将SPECAN算法用到较高分辨率成像的场合，为保证成像质量，需对是否校正二次距离弯曲进行分析。比如对采用表 1 参数的第一扫描子带，当卫星位于赤道上方且偏天地角为 30°时，由式(15) (Curlander 等，1991)可得二次距离弯曲总量约为 152.5m，即使一个 Burst 也会有 5.5 个距离门的弯曲偏移，故二次弯曲影响已不可忽略。

$$R_{\text{square}}=\frac{\lambda|f_{\text{d}r}|}{4}(t-t_0)^2\approx\frac{\lambda|f_{\text{d}r}|}{4}\left(\frac{\lambda\cdot R_c}{2Dv_{\text{s}}}\right)^2 \tag{15}$$

式中，t_0为多普勒中心频率时刻；R_{c}为波束中心视线长度；D为等效天线长度；v_{s}为卫星速度。图 5 给出上述条件下一个 Burst 数据的 SPECAN 成像结果，此例中传播路径误差已经去除。图 5(a) (b)为进行了包含二次弯曲项的距离迁徙校正后点目标成像结果，此时方位向3dB分辨率为4.5 m，距离向3dB分辨率为 4.6 m，因此点目标聚焦良好。若忽略二次弯曲，则不能实现距离、方位的解耦，点目标在方位向和距离向均不能正确聚焦。图 5(c)(d)分别显示了此时方位向和距离向剖面图，这时方位向 3dB 分辨率变为 9.3m，距离向 3dB 分辨率变为 6.3 m，且一侧旁瓣高于−7.5dB。上述仿真结果也表明若采用表 1 所示参数，则在进行距离迁徙校正必须考虑二次距离弯曲的影响，这样就使得 SPECAN 算法相对于全孔径 CS 或 RD 算法运算效率高的优势不再存在。

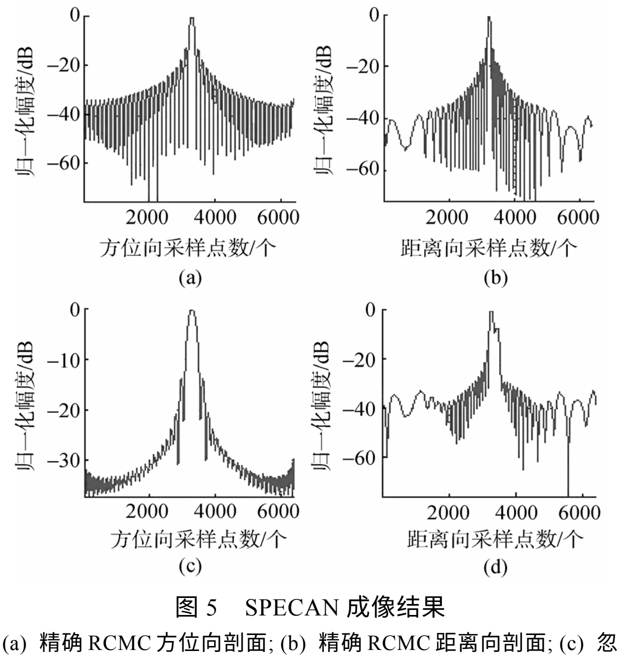

图 5　SPECAN 成像结果

(a) 精确 RCMC 方位向剖面；(b) 精确 RCMC 距离向剖面；(c) 忽略二次弯曲时方位向剖面；(d) 忽略二次弯曲时距离向剖面

因图5中横坐标均进行了64倍插值，所以距离向采样间隔为4.55/64=0.07 m。方位向采样间隔对于SPECAN算法而言可通过式(16) (Cumming 等, 2005)确定。

$$\delta_{\text{a}}=\frac{v_{\text{s}}\times \text{PRF}_{\text{e}}}{64\times N_{\text{fft}}/|f_{\text{d}r}|} \tag{16}$$

式中，v_{s}为卫星速度，PRF_{e}为等效 PRF，N_{fft}为 SPECAN 算法中方位向聚焦时每次 FFT 的长度，f_{dr}为多普勒调频率。此仿真实例中 v_{s} 为 7451.8m/s; PRF_{e}为 10080Hz; N_{fft}为 16384 点; $|f_{\text{d}r}|$为 1890.9Hz/s, 故方位向采样点间隔约为 0.04 m。归一化幅度坐标值在本文中均采用 $20\log(f/f_{\max})$求得，$f_{\max}$为幅度最大值，f为各采样点上的实际幅度值。

6.2　方位多波束所引起相位误差的仿真分析

若较好补偿了因多波束而引起的方位向相位误差，或者能保证相位误差对成像质量影响可忽略，则 MAB-ScanSAR 的处理将与普通 ScanSAR 相同。采用 4.2 节方法生成各种相位误差，利用 CS 算法进行成像分析。为避免 Burst 之间的交叉调制，在点目标分析时只是对一个有效 Burst 成像。因为偏航控制原因，非均匀采样误差影响已经很小，并且该误差随卫星所处轨道位置不同的变化不大，比如采用表 1 所示雷达参数时，对于第一扫描子带的数据，即使系统工作 PRF 偏离理想 PRF(1656 Hz) 200 Hz，也就是系统工作 PRF 为 1856 Hz (对应等效 PRF 为 11136 Hz)时，最高虚像能量与主点目标能量之比仅为 −42.5 dB (图 6(c))，故该误差对成像质量的影响完全可以忽略。

受地球自转影响，传播路径误差的影响随卫星所处位置不同有较大变化，图 6 给出了传播路径误差影响较为严重的北纬 35°处仿真结果。图 6(a)为含有混合相位误差的点目标图像方位向剖面图，此时最高虚像幅度已达−9 dB。图 6(b)为利用式(6)补偿路径差后的成像结果，此时虚像已被有效去除(最高幅度约为−42 dB)，信噪比也得到极大改善。图 6(c)为仅含有非均匀采样误差时成像结果，比较图 6(b)(c)看出，图 6(b)中的少量残余虚像主要是由非均匀采样误差引起，并且对成像质量影响可忽略。为分析方便，图 6(d)给出了不含路径差和非均匀采样误差时的成像结果。其中图 6 中横坐标采样间隔为 $v_{\text{s}}/\text{PRF}_{\text{e}}$=0.67 m。

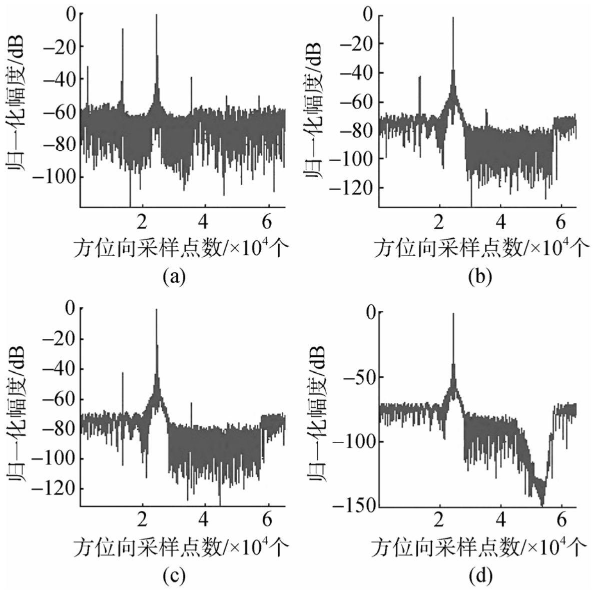

图 6 北纬 35°处方位向相位误差仿真分析

(a) 同时含有传播路径误差和非均匀采样误差; (b) 补偿(a)中传播路径误差后; (c) 只含非均匀误差时; (d) 不含相位误差时

6.3 MAB-ScanSAR 成像效果对比分析

图7给出了偏天地角为30°, 系统PRF=1680 Hz, 卫星位于赤道上方时, 条带模式, 扫描模式及补偿传播路径误差后 MAB-ScanSAR 模式点目标的成像结果。其中扫描模式为五子带单视。

图 7 中水平方向为方位向, 为方便比较, 图 7 中方位向已转化为相同的采样间隔 v_s/PRF=4.44 m。此时距离向采样间隔仍为 4.55 m。将上述成像结果的主要量化指标汇总后, 可用表 2 表示。

表 2 不同工作模式成像性能比较

工作模式	ρ_r/m	ρ_a/m	总测绘带宽/km
条带模式	4.6	4.5	69.2
扫描式	4.6	27	346
MAB-ScanSAR	4.6	4.5	346

其中, ρ_r 为距离向 3 dB 分辨率, ρ_a 为方位向 3 dB 分辨率, 总测绘带宽为斜距面不考虑子带间重叠的最佳宽度。实际系统中考虑到子带间的拼接问题, 相邻子带有一定的重叠, 故实际得到的总测绘带宽度要略小于此值(Jurgen 等, 2002; Cumming 等, 2005)。由仿真结果看出, MAB-ScanSAR 理想情况下可以实现在保持条带工作模式分辨率不变的前提下将测绘带宽扩展 5 倍。

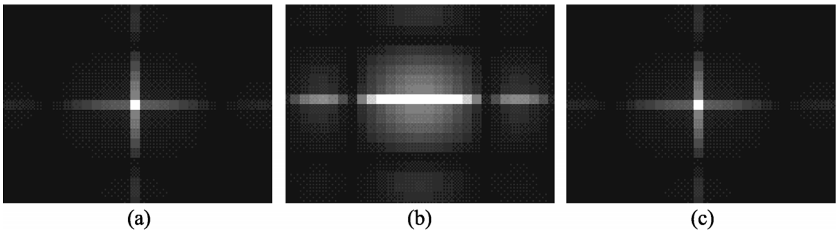

图 7 3 种工作模式的点目标灰度图像

(a) 条带式; (b) 扫描式; (c) MAB-ScanSAR

7 结 论

为了在保持较高方位分辨率的不变情况下获得更宽的测绘带, 提出了一种新型 MAB-ScanSAR 工作模式, 给出了理论上可获得的最佳性能。分析了该工作方式下的主要相位误差, 给出了具体补偿方法, 并讨论了几种适合此工作模式的成像算法。通过点目标仿真, 验证了所述方法的有效性和可行性。

REFERENCES

Andrea M G and Claudio P. 1996. ScanSAR focusing and interferometry. *IEEE Transaction on Geoscience and Remote Sensing*, **34**(4): 1029—1038

Cumming I G and Wong F H. 2005. Digital Processing of Synthetic Aperture Radar Data: Algorithms and Implementation. Norwood: Artech House Inc.

Curlander J C and Mcdonough R N.1991.Synthetic Aperture Radar: Systems and Signal Processing. New York: Wiley & Sons, Inc.

Currie A and Brown M A. 1992. Wide-swath SAR. *IEE Proceedings-F*, **139**(2): 122—135

Eldhuset K and Valand P A. 1995. ScanSAR processing and simulation for ASAR using ERS-1 raw data. *Intentional Journal of Remote Sensing*, **16**(14): 2657—2674

Gerhard K, Nicolas G and Alberto M. 2004. Unambiguous SAR signal reconstruction from nonuniform displaced phase center sampling. *IEEE Geoscience and Remote Sensing Letters*, **1**(4): 260—264

Jurgen H and Richard B. 2002. Burst mode and ScanSAR interferometry. *IEEE Transaction on Geoscience and Remote Sensing*, **40**(9): 1917—1934

Kou G J, Wang Z S and Yao P. 2009. Study on signal processing of azimuth multi-channel spaceborne SAR with yaw steering. IET International Radar Conference 2009, Guilin, China

Raney R K. 1986. Doppler properties of radars in circular orbits. *Intentional Journal of Remote Sensing*, **7**(9): 1153—1162

Sack M, Ito M R and Cumming I G.1985. Application of efficient linear FM matched filtering algorithms to synthetic aperture radar processing. IEEE Proceedings. **132**(1): 45—57

Yin C J.1997.Perfect reconstruction of digital spectrum from nonuniformly sampled signals. *IEEE Transaction on Instrumentation and Measurement*, **46**(3): 649—652